OPEN ACCESS
Journal of Innovative Optical Health Sciences
Vol. 14, No. 1 (2021) 2140009 (9 pages)

DOI: 10.1142/S1793545821400095

World Scientific
www.worldscientific.com

Swept source intraoperative OCT angiography

Ziyi Zhang*, Tiepei Zhu†, Tongtong Cao*, Zhaoyu Gong*, Lin Yao*, Kaiyuan Liu*, Juan Ye† and Peng Li*,‡,§

*State Key Lab of Modern Optical Instrumentation
College of Optical Science and Engineering
Zhejiang University, Hangzhou
Zhejiang 310027, P. R. China

†Eye center of the Second Affiliated Hospital
College of Medicine, Zhejiang University
Hangzhou, Zhejiang 310003, P. R. China

‡International Research Center for Advanced Photonics
Zhejiang University, Hangzhou
Zhejiang 310027, P. R. China
§peng_li@zju.edu.cn

Received 13 October 2020
Accepted 16 December 2020
Published 19 January 2021

To accurately guide surgical instruments during ophthalmic procedures, some necessary intraoperative depth perception is required, which standard surgical microscopes supply limitedly. Intraoperative optical coherence tomography (iOCT), combining optical coherence tomography (OCT) technology and surgical microscope, enables noninvasive, real-time and high-resolution cross-sectional imaging. Currently, though iOCT enables structural imaging, little research has been done on intraoperative angiography. In this work, we presented a swept-source intraoperative OCT angiography (SS-iOCTA) system based on a standard surgical microscope, which provides both structural and angiographic images. The feasibility of the proposed SS-iOCTA was confirmed through deep anterior lamellar keratoplasty (DALK) of *ex vivo* porcine eyes and blood perfusion imaging of *in vivo* rat cortex. High-resolution intraoperative feedback, including sub-surface structure and angiogram of biological tissue, can be visualized simultaneously with the SS-iOCTA system, which expand the surgeon's capabilities and could be widely used in clinical surgery.

Keywords: Biomedical imaging; optical coherence tomography; optical coherence tomography angiography; ophthalmology; deep anterior lamellar keratoplasty.

§Corresponding author.

1. Introduction

In order to guide surgical instruments precisely, ophthalmic procedures require some necessary intraoperative feedback in depth, while standard surgical microscopes only supply limited depth information. With the ability to perform "optical biopsy" in a noncontact, noninvasive way and provides high-resolution structural images in real-time, optical coherence tomography (OCT) has been widely used in clinical diagnosis.[1–3] Currently, the surgical microscope system integrated with OCT, termed as intraoperative optical coherence tomography (iOCT), can provide direct visualization of ophthalmic surgery in real-time.[4–7] Multiple clinical evaluations demonstrated that iOCT has the potential to improve the quality of posterior and anterior segment surgery.[8–10] Several research groups have reported methods for automatic depth measurement, surgical instruments tracking and scan axis rotation, which were further combined with heads up displays (HUDs) to guide minimally invasive ophthalmic microsurgery.[11–13] However, most intraoperative applications are limited to structural imaging because of the low contrast between capillaries and retinal tissue in OCT, which result in a lack of essential depth perception about sub-surface blood flow.

Optical coherence tomography angiography (OCTA), as a functional extension of OCT, provides noninvasive, capillary level, and unmarked 3D blood perfusion by utilizing flowing red blood cells (RBCs) as intrinsic agents.[14,15] Recent developments of high-speed OCT systems and efficient OCTA algorithms further promote the clinical practice of OCTA.[15–18] Efficient real-time angiogram generated with the aforementioned modalities provides valuable information to guide the ophthalmic surgery.[19–22]

In this study, we proposed a swept-source intraoperative OCTA (SS-iOCTA) system based on a standard surgical microscope, which provides both structural and angiographic images. The feasibility of the proposed SS-iOCTA was demonstrated with deep anterior lamellar keratoplasty (DALK) of *ex vivo* porcine eyes and blood perfusion imaging of *in vivo* rat cortex, where the SS-iOCTA visualized not only the 3D high-resolution structure and blood perfusion inside the tissue, but also the instrument-tissue interactions through surgical microscope during the surgery. The SS-iOCTA system has better capability of intraoperative monitoring and guidance, and could help surgeons make correct decisions via various surgical visualizations.

2. Materials and Methods

2.1. *SS-iOCTA system*

The surgical microscope system integrating OCT and OCTA utilized a swept frequency source (Axsun Technologies, Billerica, MA) offering the central wavelength of 1060 nm and a full width at half maximum bandwidth of 100 nm, A-scan rate of 100 kHz, sensitivity of 102 dB, range of imaging depth of ∼3.7 mm, and axial resolution of ∼7.3 μm in air. The reference arm adopted a transmissive optical path. The optical path of the sample arm was coupled with the surgical microscope [OPMI Lumera 300, Carl Zeiss Meditec, Oberkochen, Germany, see Fig. 1(b)] through the assistant microscope port of the surgical microscope. A mechanical adapter was designed to attach scanning mirrors of sample arm to surgical microscope, allowing OCT and microscope to focus simultaneously. A CCD camera was linked to the surgical microscope to capture images or record videos. A three-axis stage was placed below microscope for placing samples. The software-user interface controlling the system was self-defining. When surgeons use the SS-iOCTA system to perform a surgery, they can observe the surface of biological tissue from the software-user interface or eyepiece optionally, and observe the real-time OCT and OCTA images of the biological tissue from the software-user interface simultaneously.

2.2. *Experiment of intraoperative structural imaging*

To demonstrate the capability of SS-iOCTA to generate structural images of biological tissues, we performed a typical eye surgery (DALK) monitored by our SS-iOCTA system. Ten cadaveric porcine eyes were obtained in pairs within 2 h of enucleation and conserved in containers at 4°C before experiment. The experimental procedures in this study were in accordance to the Association for Research in Vision and Ophthalmology (ARVO) Statement for the Use of Animals in Ophthalmic and Visual Research.

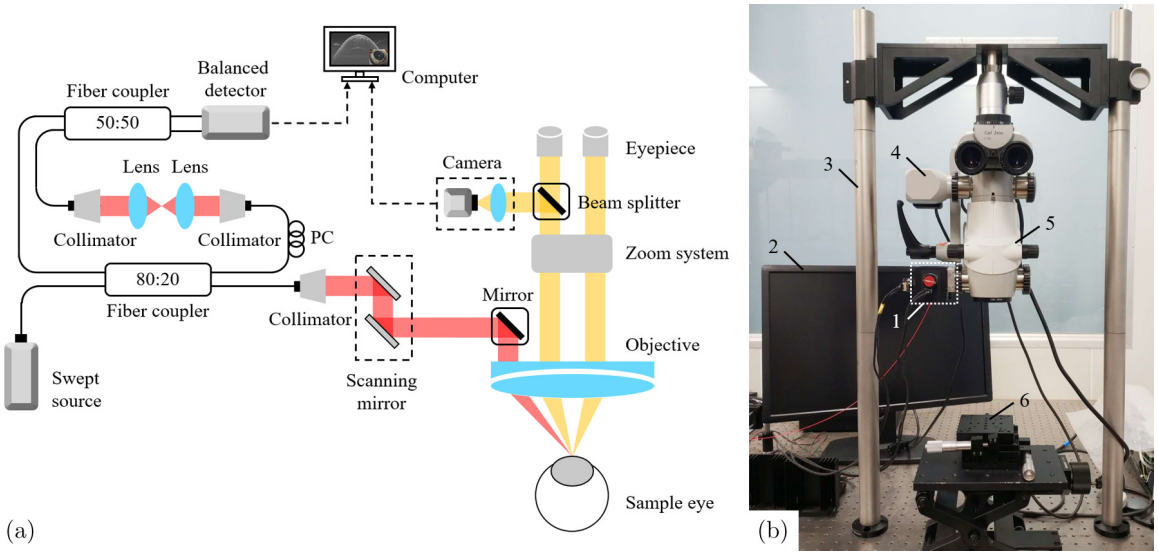

Fig. 1. The SS-iOCTA system based on a standard surgical microscope. (a) Schematic of the system setup. (b) The sample arm, computer screen and sample table (where surgeons operate) of the experimental setup. 1: scanning mirror; 2: computer screen; 3: a custom support used for fixing surgical microscope; 4: CCD camera; 5: the main body of surgical microscope; 6: three-axis stage.

DALK, an alternative to penetrating keratoplasty (PK), has advantages including the absence of allograft rejection, a shortened duration of topical corticosteroid treatment and a reduced associated risk of glaucoma, cataract, or infection. Because of those properties, the DALK is gaining popularity worldwide in the treatment of keratoconus and corneal stromal diseases in patients with healthy endothelium.[23–25] However, DALK still has a high degree of difficulty and risk of corneal perforation.[26] Using OCT to provide high-resolution images of the corneal microstructure during surgery can improve the safety of surgery and reduce the incidence of complications.[27,28]

There are numerous techniques to expose Descemet membrane (DM) during DALK, including hydro-delamination, viscoelastic dissection, and anterior chamber air injection.[29] The most appreciated technique is the big bubble, first described by Anwar and Teichmann in 2002, where a deep intrastromal air injection was used to separate DM and the overlying corneal stroma.[30]

Currently, DALK generally includes the following steps: (1) The removal of the anterior two-third stroma with trephine and corneal scissors; (2) A 27-gauge needle, keeping bevel down, is inserted into the stroma, and then advanced 3–4 mm at an angle almost parallel to the cornea from the cornea's paracentral zone to its apex; (3) Air was injected into the corneal stroma to form big bubbles and separate the stroma and DM; (4) Dissect the thin layer of stroma; (5) Suture the graft to the recipient stroma.[29–32] The feasibility experiment of DALK was conducted on 10 cadaveric porcine eyes with SS-iOCTA.

During the DALK, intraoperative structural imaging can be used to monitor the removal process to prevent the surgical instrumentation from causing corneal perforation in the first step; to help the needle tip reach the best target depth, approximately 90+% total corneal depth in the second step; to observe the state of big bubbles, and the bubbles with diameter greater than 7 mm are considered as successful in third step[29]; to determine whether DM is ideally separated from the stroma after dissecting in the fourth step (the mean value of remaining stroma's thickness in cases of successful big-bubble formation was statistically lower than failed procedures[33]); to ensure graft apposition at the end of surgery in the last step.

2.3. *Experiment of intraoperative OCT angiography*

Rat cortex imaging was performed to demonstrated the feasibility of using the SS-iOCTA system to generate *in vivo* intraoperative angiogram. Experiments were conducted on an adult male Sprague-Dawley rat (~300 g). All animal experimental procedures in this study were in accordance to the

guide for the care and use of laboratory animals from Chinese Ministry of Health and approved by Zhejiang University Animal Care and Use Committee.

The rat was anesthetized with propofol (1.5 mL/100 g) and fixed in a stereotaxic apparatus. To acquire a transparent optical window ($\sim 3 \times 3\,\mathrm{mm}^2$) on the cortex, craniotomy, and durotomy were performed to expose barrel cortex, and the location of the operation was 2–6 mm lateral to the midline and 0–4 mm posterior to the bregma. Agar in saline (1.5%) was used to cover and protect the cortex. A round glass coverslip was placed on the agar, and dental cement was used to seal the cranial window to the skull.

OCTA utilizes the relative motion of RBCs and the surrounding tissue as an endogenous marker of blood flow to replace conventional exogenous fluorescent markers, and visualizes noninvasive, capillary level, and unmarked 3D vasculature and perfusion. The 3D flow data in specific tissue layers or slabs can be compressed into one 2D *en face* image to represent the vasculature and perfusion intuitively.[15,16,34] Compared with fundus photography that can only image the surface of vessels, OCTA results from RBCs motion can visualize the perfusion, which meet the needs of locating pathologic vessels precisely in ophthalmic procedures.[20–22]

To accurately distinguish dynamic blood flow regions and static surrounding tissues, the inverse signal-to-noise ratio (iSNR)-decorrelation OCTA (ID-OCTA) algorithm was used in this study, where a classification line was set in ID space along the 3σ boundary of the distribution of static signals to remove the static tissues.[34]

During this demonstrative experiment of intraoperative OCTA, we scanned the whole transparent optical window where the typical vessels in rat cortex can be observed by SS-iOCTA. The diameter of retinal arterioles ($\sim$150 μm) and venules ($\sim$200 μm) in normal human subjects,[35] which are similar to the diameter of typical vessels in rat cortex. Therefore, the vessels of *in vivo* rat cortex were selected as the feasibility experiment sample in this study, and the ID-OCTA algorithm was used to visualize the map of vasculature.

3. Results

3.1. *Results of intraoperative structural imaging*

DALK was performed on 10 cadaveric porcine eyes with SS-iOCTA following the steps described in Sec. 2.1. As shown in Fig. 2, in these representative steps, intraoperative OCT shows the structural

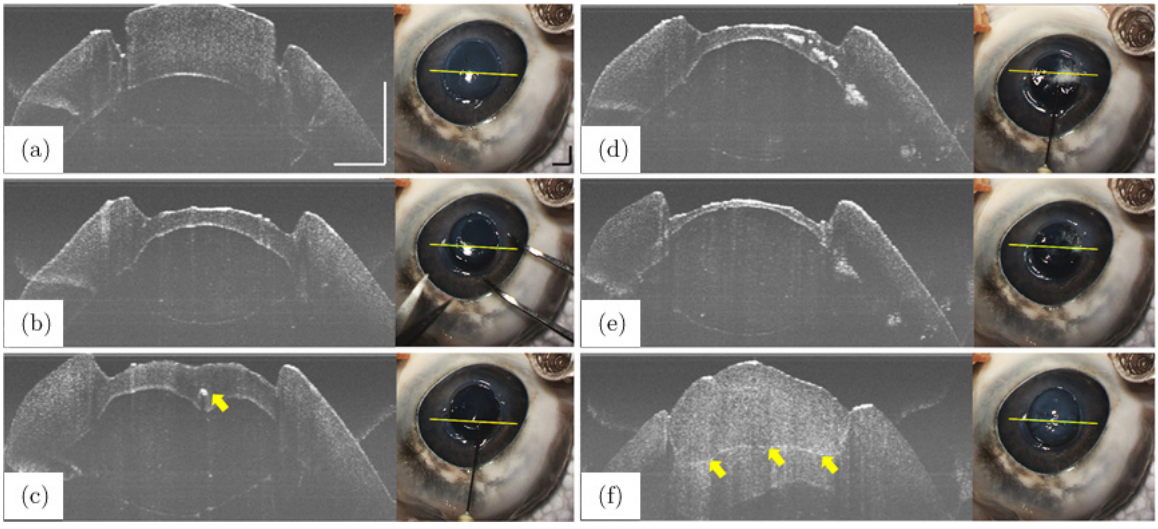

Fig. 2. The typical procedures of DALK, performed on cadaveric porcine eye with SS-iOCTA, were captured by OCT and CCD camera simultaneously. (a) The corneal stroma after trephine cut. (b) The anterior two thirds of the stroma was removed. (c) Insert the needle into stroma, and the arrow indicates the position of the needle tip. (d) After injecting air into the corneal stroma, some diffuse small bubbles were formed, as shown by the high scattering signal in the corneal stroma. (e) After dissecting the residuary part of stroma, the remnant was thin enough to place the graft. (f) The arrows indicate the boundary between graft and recipient stroma, which shows both fit fully. The yellow line in every image of surgical microscope is virtual aiming beam representing the scanning position (B-scan) of OCT. All images in Fig. 2 are from the real-time SS-iOCTA video during DALK. Scale bar: 2 mm.

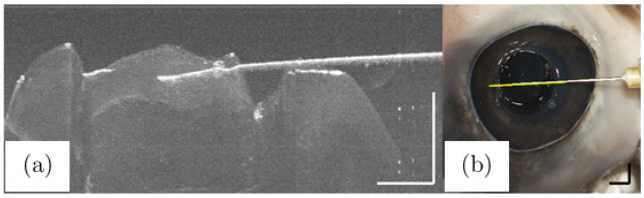

Fig. 3. Insert the needle into stroma from the direction parallel to the virtual aiming beam after removing the anterior two thirds of the stroma. (a) The maximum intensity projections of the 3D results from OCT. (b) The image captured by CCD camera. Scale bar: 2 mm.

cross section in real-time, including the shape of the front surface, the back boundary and scatter signal of corneal stroma. According to the capability of depth perception mentioned above, valuable feedback can be explicitly obtained as follows: the depth of trephine entry, the position especially the depth of needle, the status of bubbles, the thickness of remaining stroma, and the boundary line between graft and recipient stroma.

Additionally, if the needle is inserted into corneal stroma from the direction parallel to the scanning position (B-scan) of OCT, metallic surgical instrumentation would partly block the ray of OCT and form shadow below. In that case, some critical structural information below the instrument probably gets lost such as the shape of front and back boundaries of stroma. Therefore, we performed 3D scan in a small range (about 1 mm perpendicular to the cross-section) and display the maximum intensity projections of the 3D results in real-time when the needle was parallel to the B-scan of OCT (refer to Fig. 3). This method has optimized the cross-sectional view that shows the instrument-tissue interaction when shadow was caused by surgical instruments, on the grounds that the tissue shadowed underneath the needle should be similar to surrounding tissue because of the smoothness of cornea.

3.2. *Results of OCTA*

The results of the feasibility experiment demonstrate that the blood perfusion including large vessels and their branches in rat cortex can be visualized by OCTA. With 300 A-scans per B-scan, 2 repeated B-scans (in x direction) per lateral location and 300 lateral locations (in y direction) per 3D data, the OCTA scan was completed in ∼2.3 s. The distribution of static and dynamic OCT signals was generated by ID-OCTA algorithm as shown in Fig. 4(a). A classification lines removed the OCT signals representing the static surrounding tissues while the others were retained as dynamic signals.[34] By reconstruction and projection, 2D *en face* image of OCTA containing dynamic signals of the whole 3D data was further achieved [Fig. 4(b)]. The vasculature between the results from OCTA and surgical microscope correspond in position and morphology. Moreover, it is blood perfusion of typical *in vivo* vessels that the *en face* OCTA represents while the image captured by CCD camera of surgical microscope shows the surface of corresponding vessels.

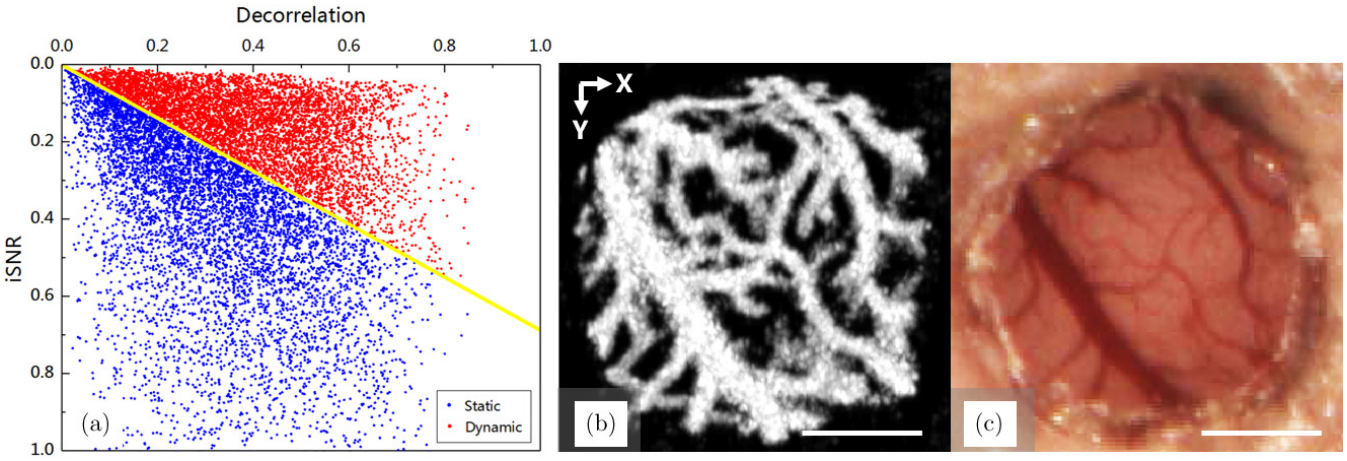

Fig. 4. The results of the feasibility experiment of OCTA. (a) The distribution of OCT signals, where the signals marked with blue represent the static surrounding tissues while the dynamic signals were marked with red. The yellow line is the classification lines generated by ID-OCTA algorithm. (b) The 2D *en face* image of OCTA. (c) The image of optical imaging window captured by CCD camera of surgical microscope. Scale bar: 1 mm.

4. Discussion

High-resolution intraoperative imaging can be visualized simultaneously by this SS-iOCTA system, including 3D structural and angiographic images that cannot be acquired with standard surgical microscope. At present, iOCT has been developed in OCT scanning direction, imaging speed and automatic tracking,[11–13] but current intraoperative applications are limited to structural imaging. Actually, intraoperative angiography offers monitoring and guidance in surgery related to blood perfusion, especially laser therapy. For example, intraoperative real-time angiography helps to position the laser accurately in the nonperfusion area or in retinal neovascularization (RNV) area during laser therapy, while the traditional method that surgeons locate laser according to the preoperative fluorescein angiography may cause positioning deviation.[20–22] Considering the demands of intraoperative angiographic imaging in ophthalmic procedures as mentioned above, we have integrated OCTA technology with iOCT system. With the help of intraoperative OCTA refreshed per few seconds, the target location in retinal vasculature will be found and monitored more accurately than with traditional method. A research on OCTA with Microscope-Integrated Optical Coherence Tomography (MIOCT) system has been reported, where retinal angiograms of two children was acquired successfully several months after the surgery.[19,36] However, this MIOCT system requires a sophisticated modification of the original hardware of Leica M841, which is not universally appliable to other systems. Compared to MIOCT, a mechanical adapter of SS-iOCTA system was designed to attach OCTA module to surgical microscope through the standard assistant microscope port. With the design of adapter, OCTA module could be installed conveniently and provide better universality. Furthermore, according to the demos in our report, iOCT and iOCTA can support essential intraoperative imaging not only in ophthalmic procedures, but also in neurosurgery or other surgical disciplines.

While our structural imaging from the DALK were encouraging, we recognized that there were some limitations in our experimental design. Even if the needle tip reaches its best position, some diffuse small bubbles were formed instead of the big bubble [Fig. 2(d)]. This could be caused by significant endothelium cell loss in the porcine eyes we acquired after enucleation, shown by cornea clouding.[37,38] Moreover, we only used the SS-iOCTA system to perform DALK of 10 porcine eyes instead of comparative experiments containing the more cases with/without SS-iOCTA. In the future work, DALK will be considered for *in vivo* human eyes or human corneal graft, and comparative experiments will be designed to demonstrate the advantages of SS-iOCTA statistically with the parameters such as perforation rates, insertion depth and so on.

Although the OCTA results we got using the system visualized the blood perfusion of rat cortex, its resolution needs to be improved. The possible reason for this was that the optical path of OCT passing through the galvanometer was directly folded from the mirror of surgical microscope to the objective lens (the focal length is up to 200 mm). According to the theory of the diffraction limit, larger focal length results in larger Airy disk diameter, which will make the lateral resolution of the OCT image worse, and further limit the resolution of OCTA. In the follow-up work, it is worth to optimize the optical path of the system, such as adding relay lenses to the OCT sample arm to improve the lateral resolution.

Additionally, the artifacts of intraoperative OCTA also need to be considered. In the clinical application of intraoperative, motion artifacts resulting from eye movements can be eliminated by fixation of eye during surgery, eye tracking systems and motion correction technology; projection artifacts in deeper retinal layers resulting from the multiple scattering effects of superficial vasculature can be removed by algorithms in reconstruction.[14,39,40] To optimize the results of imaging, the problems of artifacts in intraoperative OCTA could be overcome by a means combining the above methods and the demands of surgery in the follow-up work.

Besides, the swept source offering A-scan rate up to MHz scale could be used to acquire 3D imaging with higher rate, and the graphics processing unit (GPU) could be used to reconstruct the structural and angiographic imaging results in real-time.[41,42] With the higher speed acquisition and data processing by GPU, real-time intraoperative OCTA in human eyes during experimental surgery is expected.

5. Conclusion

In this report, we presented a SS-iOCTA system for both the structural and angiographic imaging based on a standard surgical microscope. DALK of *ex vivo* porcine eyes was used to demonstrate the intraoperative OCT structural imaging while blood perfusion imaging of *in vivo* rat cortex was the feasibility experiment of intraoperative OCTA. High-resolution sub-surface structure, blood perfusion, as well as the instrument–tissue interactions could meet the need of intraoperative depth perception. The proposed SS-iOCTA system could help surgeons make correct decisions and be applied in clinical surgery broadly.

Conflicts of Interest

The authors have no conflicts of interest relevant to this article.

Acknowledgment

National Natural Science Foundation of China (62075189 and 81873911), Zhejiang Provincial Natural Science Foundation of China (LR19F050002), Zhejiang Lab (2018EB0ZX01), Fundamental Research Funds for the Central Universities (2018FZA5003).

References

1. D. Huang, E. A. Swanson, C. P. Lin, J. S. Schuman, W. G. Stinson, W. Chang, M. R. Hee, T. Flotte, K. Gregory, C. A. Puliafito *et al.*, "Optical coherence tomography," *Science* **254**(5035), 1178–1181 (1991).
2. J. A. Izatt, M. R. Hee, E. A. Swanson, C. P. Lin, D. Huang, J. S. Schuman, C. A. Puliafito, J. G. Fujimoto, "Micrometer-scale resolution imaging of the anterior eye in vivo with optical coherence tomography," *Arch. Ophthalmol.* **112**(12), 1584–1549 (1994).
3. C. A. Puliafito, M. R. Hee, C. P. Lin, E. Reichel, J. S. Schuman, J. S. Duker, J. A. Izatt, E. A. Swanson, J. G. Fujimoto, "Imaging of macular diseases with optical coherence tomography," *Ophthalmology* **102**(2), 217–229 (1995).
4. J. P. Ehlers, "Intraoperative optical coherence tomography: Past, present, and future," *Eye* **30**(2), 193–201 (2016).
5. J. P. Ehlers, J. Goshe, W. J. Dupps, P. K. Kaiser, R. P. Singh, R. Gans, J. Eisengart, S. K. Srivastava, "Determination of feasibility and utility of microscope-integrated optical coherence tomography during ophthalmic surgery: The DISCOVER Study RESCAN Results," *JAMA Ophthalmol.* **133** (10), 1124–1132 (2015).
6. M. Pfau, S. Michels, S. Binder, M. D. Becker, "Clinical experience with the first commercially available intraoperative optical coherence tomography system," *Ophthalmic Surg. Lasers Imaging Retina* **46**(10), 1001–1008 (2015).
7. Z. Yang, J. Shang, C. Liu, J. Zhang, F. Hou, Y. Liang, "Intraoperative imaging of oral-maxillofacial lesions using optical coherence tomography," *J. Innov. Opt. Health Sci.* **13**(2), 2050010 (2020).
8. J. Au, J. Goshe, W. J. Dupps, Jr. S. K. Srivastava, J. P. Ehlers, "Intraoperative optical coherence tomography for enhanced depth visualization in deep anterior lamellar keratoplasty from the PIONEER study," *Cornea* **34**(9), 1039–1043 (2015).
9. P. Hahn, J. Migacz, R. O'Donnell, S. Day, A. Lee, P. Lin, R. Vann, A. Kuo, S. Fekrat, P. Mruthyunjaya, E. A. Postel, J. A. Izatt, C. A. Toth, "Preclinical evaluation and intraoperative human retinal imaging with a high-resolution microscope-integrated spectral domain optical coherence tomography device," *Retina* **33**(7), 1328–1337 (2013).
10. J. P. Ehlers, W. J. Dupps, P. K. Kaiser, J. Goshe, R. P. Singh, D. Petkovsek, S. K. Srivastava, "The prospective intraoperative and perioperative ophthalmic imaging with optical coherence tomography (PIONEER) Study: 2-year results," *Am. J. Ophthalmol.* **158**(5), 999–1007.e1 (2014).
11. Y. K. Tao, S. K. Srivastava, J. P. Ehlers, "Microscope-integrated intraoperative OCT with electrically tunable focus and heads-up display for imaging of ophthalmic surgical maneuvers," *Biomed. Opt. Exp.* **5**(6), 1877–1885 (2014).
12. B. Keller, M. Draelos, G. Tang, S. Farsiu, A. N. Kuo, K. Hauser, J. A. Izatt, "Real-time corneal segmentation and 3D needle tracking in intrasurgical OCT," *Biomed. Opt. Exp.* **9**(6), 2716–2732 (2018).
13. O. M. Carrasco-Zevallos, B. Keller, C. Viehland, L. Shen, G. Waterman, B. Todorich, C. Shieh, P. Hahn, S. Farsiu, A. N. Kuo, C. A. Toth, J. A. Izatt, "Live volumetric (4D) visualization and guidance of in vivo human ophthalmic surgery with intraoperative optical coherence tomography," *Sci. Rep.* **6**, 31689 (2016).
14. C.-L. Chen, R. K. Wang, "Optical coherence tomography based angiography [Invited]," *Biomed. Opt. Exp.* **8**(2), 1056–1082 (2017).

15. R. F. Spaide, J. G. Fujimoto, N. K. Waheed, S. R. Sadda, G. Staurenghi, "Optical coherence tomography angiography," *Prog. Retinal Eye Res.* **64**, 1 (2018).
16. A. M. Hagag, S. S. Gao, Y. Jia, D. Huang, "Optical coherence tomography angiography: Technical principles and clinical applications in ophthalmology," *Taiwan J. Ophthalmol.* **7**(3), 115–129 (2017).
17. C. Posarelli, F. Sartini, G. Casini, A. Passani, M. D. Toro, G. Vella, M. Figus, "What is the impact of intraoperative microscope-integrated OCT in ophthalmic surgery? relevant applications and outcomes. a systematic review," *J. Clin. Med.* **9**(6), 1682 (2020).
18. R. F. Spaide, J. Klancnik, M. J. Cooney, "Retinal vascular layers imaged by fluorescein angiography and optical coherence tomography angiography," *JAMA Ophthalmology* **133**(1), 45–50 (2015).
19. X. Chen, C. Viehland, O. M. Carrasco-Zevallos, B. Keller, L. Vajzovic, J. A. Izatt, C. A. Toth, "Microscope-integrated optical coherence tomography angiography in the operating room in young children with retinal vascular disease," *JAMA Ophthalmol.* **135**(5), 483–486 (2017).
20. C. Y. Chung, H. H. Y. Tang, S. H. Li, K. K. W. Li, "Differential microvascular assessment of retinal vein occlusion with coherence tomography angiography and fluorescein angiography: A blinded comparative study," *Int. Ophthalmol.* **38**(3), 1119–1128 (2018).
21. I. Kozak, J. K. Luttrull, "Modern retinal laser therapy," *Saudi J. Ophthalmol.* **29**(2), 137–146 (2015).
22. P. Kumar, Y. R. Sharma, P. Chandra, R. Azad, G. G. Meshram, "Comparison of the safety and efficacy of intravitreal ranibizumab with or without laser photocoagulation versus dexamethasone intravitreal implant with or without laser photocoagulation for macular edema secondary to branch retinal vein occlusion," *Folia Med. (Plovdiv)* **61**(2), 240–248 (2019).
23. V. Romano, A. Iovieno, G. Parente, A. M. Soldani, L. Fontana, "Long-term clinical outcomes of deep anterior lamellar keratoplasty in patients with keratoconus," *Am. J. Ophthalmol.* **159**(3), 505–511 (2015).
24. Y. Y. Cheng, N. Visser, J. S. Schouten, R. J. Wijdh, E. Pels, H. van Cleynenbreugel, C. A. Eggink, M. J. Zaal, W. J. Rijneveld, R. M. Nuijts, "Endothelial cell loss and visual outcome of deep anterior lamellar keratoplasty versus penetrating keratoplasty: A randomized multicenter clinical trial," *Ophthalmology* **118**(2), 302–309 (2011).
25. V. M. Borderie, O. Sandali, J. Bullet, T. Gaujoux, O. Touzeau, L. Laroche, "Long-term results of deep anterior lamellar versus penetrating keratoplasty," *Ophthalmology* **119**(2), 249–255 (2012).
26. Y. Tao, M. LaBarbera, J. P. Ehlers, S. K. Srivastava, W. J. Dupps, "Image-guided modified deep anterior lamellar keratoplasty (DALK) corneal transplant using intraoperative optical coherence tomography," *Investigative Ophthalmology & Visual Science* **56**(7), 1966–1966 (2015).
27. P. Steven, C. Le Blanc, E. Lankenau, M. Krug, S. Oelckers, L. M. Heindl, U. Gehlsen, G. Huettmann, C. Cursiefen, "Optimising deep anterior lamellar keratoplasty (DALK) using intraoperative online optical coherence tomography (iOCT)," *Br. J. Ophthalmol.* **98**(7), 900–904 (2014).
28. L. De Benito-Llopis, J. S. Mehta, R. I. Angunawela, M. Ang, D. T. H. Tan, "Intraoperative anterior segment optical coherence tomography: A novel assessment tool during deep anterior lamellar keratoplasty," *Am. J. Ophthalmol.* **157**(2), 334–341.e3 (2014).
29. N. D. Pasricha, C. Shieh, O. M. Carrasco-Zevallos, B. Keller, D. Cunefare, J. S. Mehta, S. Farsiu, J. A. Izatt, C. A. Toth, A. N. Kuo, "Needle depth and big-bubble success in deep anterior lamellar keratoplasty: An ex vivo microscope-integrated OCT study," *Cornea* **35**(11), 1471–1477 (2016).
30. M. Anwar, K. D. Teichmann, "Big-bubble technique to bare descemet's membrane in anterior lamellar keratoplasty," *J. Cataract Refractive Surg.* **28**(3), 398–403 (2002).
31. M. Draelos, G. Tang, B. Keller, A. Kuo, K. Hauser, J. A. Izatt, "Optical coherence tomography guided robotic needle insertion for deep anterior lamellar keratoplasty," *IEEE Trans. Bio-med. Eng.* **67**(7), 2073–2083 (2020).
32. F. Luengo-Gimeno, D. T. Tan, J. S. Mehta, "Evolution of deep anterior lamellar keratoplasty (DALK)," *Ocular Surf.* **9**(2), 98–110 (2011).
33. V. Scorcia, M. Busin, A. Lucisano, J. Beltz, A. Carta, G. Scorcia, "Anterior segment optical coherence tomography-guided big-bubble technique," *Ophthalmology* **120**(3), 471–476 (2013).
34. L. Huang, Y. Fu, R. Chen, S. Yang, H. Qiu, X. Wu, S. Zhao, Y. Gu, P. Li, "SNR-adaptive OCT angiography enabled by statistical characterization of intensity and decorrelation with multi-variate time series model," *IEEE Trans. Med. Imaging* **38**(11), 2695–2704 (2019).
35. Y. Zong, L. Lin, C. Yi, X. Huang, Y. Fu, Y. Dong, X. Qian, Y. Li, Q. Gao, "Retinal vessel oxygen saturation and vessel diameter in retinitis pigmentosa at various ages," *Graefe's Arch. Clin. Exp. Ophthalmol.* **254**(2), 243–252 (2016).
36. Y. K. Tao, J. P. Ehlers, C. A. Toth, J. A. Izatt, "Intraoperative spectral domain optical coherence

tomography for vitreoretinal surgery," *Opt. Lett.* **35**(20), 3315–3317 (2010).
37. M. Bhogal, C. N. Lwin, X.-Y. Seah, E. Murugan, K. Adnan, S.-J. Lin, G. Peh, J. S. Mehta, "Real-time assessment of corneal endothelial cell damage following graft preparation and donor insertion for DMEK," *PloS One* **12**(10), e0184824–e0184824 (2017).
38. S.-W. Teng, H.-Y. Tan, J.-L. Peng, H.-H. Lin, K. H. Kim, W. Lo, Y. Sun, W.-C. Lin, S.-J. Lin, S.-H. Jee, P. T. C. So, C.-Y. Dong, "Multiphoton autofluorescence and second-harmonic generation imaging of the ex vivo porcine eye," *Investig. Ophthalmol. Vis. Sci.* **47**(3), 1216–1224 (2006).
39. M. F. Kraus, B. Potsaid, M. A. Mayer, R. Bock, B. Baumann, J. J. Liu, J. Hornegger, J. G. Fujimoto, "Motion correction in optical coherence tomography volumes on a per A-scan basis using orthogonal scan patterns," *Biomed. Opt. Exp.* **3**(6), 1182–1199 (2012).
40. M. Zhang, T. S. Hwang, J. P. Campbell, S. T. Bailey, D. J. Wilson, D. Huang, Y. Jia, "Projection-resolved optical coherence tomographic angiography," *Biomed. Opt. Exp.* **7**(3), 816–828 (2016).
41. X. Wei, A. Camino, S. Pi, T. T. Hormel, W. Cepurna, D. Huang, J. C. Morrison, Y. Jia, "Real-time cross-sectional and en face OCT angiography guiding high-quality scan acquisition," *Opt. Lett.* **44**(6), 1431–1434 (2019).
42. X. Wei, T. T. Hormel, Y. Guo, T. S. Hwang, Y. Jia, "High-resolution wide-field OCT angiography with a self-navigation method to correct microsaccades and blinks," *Biomed. Opt. Exp.* **11**(6), 3234–3245 (2020).